How Metal Coordination in the Ca-, Ce-, and Eu-Containing Methanol Dehydrogenase Enzymes Can Influence the Catalysis: A Theoretical Point of View

Tiziana Marino, Mario Prejanò and Nino Russo

Abstract Methanol dehydrogenase (MDH) enzymes are quinoproteins that require calcium or magnesium ion as well as pyrroloquinoline quinone as a cofactor for activity in the oxidation of methanol to formaldehyde. Lately, MDH enzymes containing lanthanide ions in the active site have been isolated in drastic conditions from *Methylacidiphilum fumariolicum* bacterium. The present theoretical study performed in the framework of the density functional theory employing the quantum mechanical cluster approach mainly focused on the catalytic mechanism of cerium containing MDH enzyme. In order to rationalize the effect of the metal ion substitution on the catalytic activity, geometrical and electronic properties of the "Michaelis–Menten" enzyme–methanol complexes of Ce-MDH and Eu-MDH are also discussed as well as the substrate's activation mediated by the metal ion. With the aim to better describe the Lewis acidity of metal ions in the methanol oxidation, the comparison of the catalytic performance between Ce-MDH and Ca-MDH was also made.

1 Introduction

Metal ions are ubiquitous and widely distributed in nature and account extremely important roles in chemistry, geochemistry, biochemistry, material sciences, and medicine. Approximately one-third of the structures in the Protein Data Bank (PDB) contains metal ions.

Metals such as copper (Cu), iron (Fe), lanthanides (Ln), cobalt (Co), zinc (Zn), molybdenum (Mo), and tungsten (W) are particularly important for methanotrophy [1].

In particular, rare earth elements (REE) including lanthanum and lanthanoid (17 elements) as well as scandium and yttrium are found in bacteria, archaebacteria, fungi, vegetables, and animals [2]. They are known to act as calcium analogs in the

T. Marino (✉) · M. Prejanò · N. Russo
Dipartimento di Chimica e Tecnologie Chimiche, Università della Calabria, 87036 Rende, Italy
e-mail: tiziana.marino65@unical.it

E. Broclawik et al. (eds.), *Transition Metals in Coordination Environments*,
Challenges and Advances in Computational Chemistry and Physics 29,
https://doi.org/10.1007/978-3-030-11714-6_16

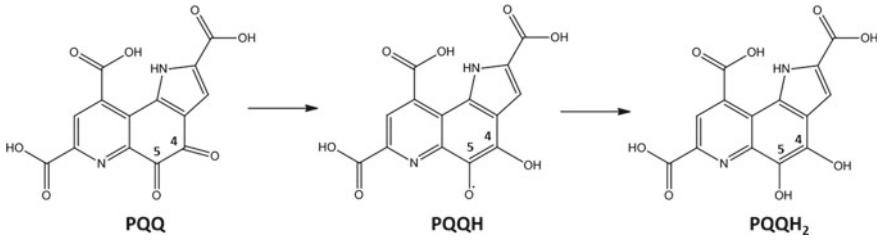

Scheme 1 Three different oxidation states of the pyrroloquinoline quinone during the methanol oxidation by MDH enzyme

biological systems, and in particular, lanthanum ions (III) may replace calcium in many proteins including enzymes [3, 4].

REE were considered for long time to be biologically inert but very recently received a great attention since revealed to be essential metals for activity and expression of a special type of methanol dehydrogenase, XoxF. This gene, first discovered in 1995 [5, 6], is associated with the activity of a novel methanol dehydrogenase (MDH) in a methylotrophic bacterium *Methylobacterium radiotolerans* [7]. XoxF sequences share almost 50% amino acid residues with those of MxaF, the extensively studied and well-characterized two-subunit methanol dehydrogenase, that contains 2,7,9-tricarboxypyrroloquinoline quinone (PQQ) and Ca^{2+} ion as cofactors in its catalytic center [8, 9].

PQQ cofactor accepts formally two electrons and two protons from the alcohol substrate to give rise the corresponding aldehyde and the reduced form $PQQH_2$ form [10, 11]; see Scheme 1. The presence in the REE-MDH active site of an ion with larger size and higher charge compared to calcium ion requires a further amino acid residue, the Asp 301, to balance the excess of positive charge of the metal center [1, 12].

In nature, the ability of methylotrophic microorganisms to use reduced C1 compounds, such as methane and methanol, as an energy source, is a significant biological and geochemical process involved in the global carbon cycle. In the case of methanotrophic species, instead, the methane must be oxidized to methanol by a methane monooxygenase [13–15]. Studies performed on methanotrophic and methylotrophic bacteria demonstrated that they carry both MxaF and XoxF genes, but the environment plays a crucial role in their expression [16].

The XoxF REE-MDH that uses different metal ions can be considered an example of enzyme condition promiscuity where the enzyme can show catalytic activity in reaction conditions different from their natural ones. In fact, REE-MDH from SolV operates at neutral pH, whereas the Ca-MDH displays its highest activity at higher pH values [1, 17, 18].

The isolation of the XoxF-type MDH from the extremophile *Methylacidiphilum fumariolicum* SolV bacterium cultivated with mudpot water in the Solfatara crater in south Italy, allowed to identify in the active center the most abundant lanthanide, the cerium element [18]. Recently, the cultivation and purification of the strictly REE-

dependent methanotrophic bacterium SolV with europium have been also reported [19].

Despite the mechanism of methanol oxidation by calcium-containing enzyme has attracted the attention in the last 40 years and different mechanistic proposals have been suggested and discussed, today controversial opinions are present and the debate is still open [20–28]. In the case of REE-MDH, owing to the most recent discoveries [7, 14, 19, 29–31], the discussion is just beginning.

Furthermore, a deeper investigation on the reaction mechanism of cerium containing MDH has been performed by employing the quantum chemical cluster methodology in the framework of density functional theory (DFT).

Having in mind that the coordination chemistry of the lanthanides can generate structural diversity depending on the progressive decrease in ionic radius, in the present work, we present the results obtained by the comparative DFT analysis of the catalytic behavior of the cerium- and europium-containing methanol dehydrogenase. In particular, the step of the enzymatic mechanism where the metal ion plays a critical role has been considered. Both cerium and europium metal ions act as good Lewis acids in the enzyme–substrate complex (ES), and our study is focused on this step and the analysis of the structural, electronic properties and of the charges distribution can contribute to gain a more comprehensive knowledge of this important event. In addition, during the discussion, the catalytic behavior of the cerium-containing enzyme is compared with that of the more usual calcium-containing enzyme.

2 Computational Methods

2.1 Active Site Model

For the cerium enzyme, the ES starting structure has been obtained by modeling the X-ray structure of the Xoxf-type natural cerium-dependent MDH (PDB: 4MAE, 1.6 Å) [18]. It corresponds to the precatalytic enzyme–substrate complex where the polyethylene glycol instead of the natural substrate prevents the occurrence of the reaction. In the case of the Eu-MDH-used structure, the achieved crystals report the enzyme without substrate. (PDB: 6FKW, 1.4 Å) [19].

The QM cluster includes the amino acid residues of the inner coordination shell of Ce^{3+} ion (Glu172, Asn256, Asp299, Asp301) and the cofactor PQQ and Glu55, Arg110, Ser169, Arg326, Asp388 residues of the outer coordination shell that potentially form hydrogen bonds with the cofactor. All amino acids were truncated at the α carbons, and hydrogen atoms were added manually. The methanol substrate is coordinated to the metal center by the hydroxyl group. The overall model consists of 113 atoms, including the substrate, and has a total charge of zero (Fig. 1).

As usual in the cluster approach for modeling enzymatic reactions [23, 32–37], the truncated amino acid residues at the periphery of the active site are fixed to

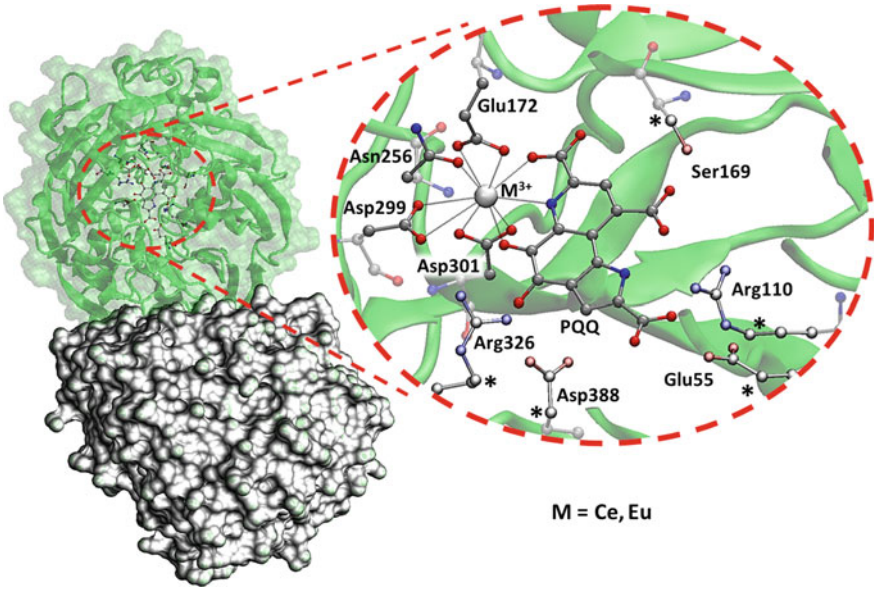

Fig. 1 Overall structure of Ce- and Eu-MDH and close-up view of the active site that shows the model cluster (in ball and stick) representing the active site of. Stars indicate the locked atoms frozen during the calculations

their crystallographic positions during the geometry optimizations. This precludes the artificial expansion of the cluster.

2.1.1 Technical Details

All the computations have been performed employing the Gaussian 09 program [38] with the Becke exchange and the Lee, Yang, Parr correlation (B3LYP) hybrid density functional method [39, 40]. Geometries have been optimized using the 6-31+G(d,p) basis set for the C, N, O, H atoms, and the SDD [41] effective core potential (ECP) coupled with its related basis set for the lanthanides. The D3 dispersions contribution [42] as implemented in the Gaussian package has been considered.

The employed relativistic effective core potential (ECP) [41] based on a number of 30 and 35 valence electrons for cerium and europium, respectively, ensures a better description of the coordination chemistry of these elements. The nature of minima (without imaginary frequency) or maxima (only one imaginary frequency) of every stationary point intercepted along the PES has been determined by frequency calculations. To estimate the energetic effects of the protein environment, single-point calculations by using the polarizable continuum method (C-PCM) coupled to the dielectric constant value $\varepsilon = 4$ have been performed [43, 44]. This value usually represents a good choice of protein surrounding [32, 34, 45–53].

For Ce-MDH, further calculations with $\varepsilon = 24$ and $\varepsilon = 78$ have been also done to test the influence of the more polar environments on its catalytic activity.

More accurate energies with the larger basis set 6-311+G(2d,2p) for all atoms except for the metal ion described by ECP have been obtained by single-point calculations performed on the optimized structures.

The given energies presented are corrected for ZPE, solvation, and dispersion effects. The same computational protocol has been successfully used in the mechanistic studies of other metal proteins [33, 34, 47, 51, 53, 54].

As far as the cerium-containing enzyme is concerned, the doublet spin multiplicity ($2S + 1 = 2$) previously determined [53, 55] has been considered as the ground state in all the calculations by using spin-unrestricted wavefunctions. Almost no spin contaminations have been evidenced due to the $\langle S\hat{}2\rangle$ value equal to 0.77.

Natural bond orbital (NBO) analysis [56] was performed on all the intercepted stationary points of the investigated PESs.

3 Results and Discussion

3.1 Ce-MDH PES

Different mechanisms have been proposed for MDH enzymes over the years [9, 18, 20, 21, 23, 27, 28, 30, 53, 57], but the exact oxidation mechanism of CH_3OH by MDH is still under debate.

In the investigated mechanism shown in Scheme 2, we propose the metal ion, during the first step evidenced in the rectangular box, to facilitate the nucleophile attack of OH group of the coordinated methanol that with its lone pair oriented toward the PQQ is preparing to transfer the proton to the Asp299 base. As a result, the O5 of PQQ coordinated to the metal ion completes the activation role played by the metal ion making C5 more suitable for the nucleophilic addition. Successively, the reaction proceeds with the protonation of the O4 of PQQ with simultaneous CH_2O formation (TS2) and then the H^+ abstraction from Asp299 with the formation of $PQQH_2$ (TS3). Summarizing during the oxidation of methanol to formaldehyde, the PQQ cofactor suffers a reduction in two steps (Scheme 1): from PQQ (starting point) to semiquinone PQQH (intermediate) and the fully reduced $PQQH_2$ form.

During the redox cycling of the PQQ cofactor, it was demonstrated the metal ion to retain the same oxidation state equal to +3 [55].

As reported in our previous works on methanol dehydrogenase enzymes [23, 53], the PESs have been obtained considering the polarization effects caused by the portion of the surrounding enzyme that is not explicitly included in the quantum model by cavity techniques. Other than the environment simulated with $\varepsilon = 4$, in the present investigation, single-point calculations with other dielectric constant values have been performed. In this way, a set of three different dielectric constants ($\varepsilon = 4$, $\varepsilon = 24$ and $\varepsilon = 78$) characterized by a trend of increasing polarity have been tested.

The results shown in Fig. 2 clearly show the absence of relevant effects in both minima and transition states as a function of the dielectric constants. Only in the case of the INT1 species, a major stabilization, by few kcal/mol, can be observed. This behavior can be ascribed to the fact that the INT1 species is the result of a series of rearrangements accomplished by different charge distributions. The absence of large solvent effects is usually related to the "completeness" of the QM selected model that already explicitly includes most of the polarization effects. The rate determining step is localized in the second part of the process (INT1 → TS2_A → INT2_A). The corresponding calculated barrier values are 19.4, 21.2, and 21.5 kcal/mol with $\varepsilon = 4$, $\varepsilon = 24$ and $\varepsilon = 78$, respectively. During this step, the produced formaldehyde is moved outside of the inner coordination shell of the metal ion and is kept close to the cerium by H-bond with Ser169 (2.020 Å).

The next step (INT2_A → TS3_A → EP) describes the restoration of the protonation state of the Asp299 residue acting as acid–base and the consequent protonation of the C5-O5$^{(-)}$ moiety. The barriers for this hydrogen transfer independently of the simulated environments (5.4 kcal/mol for $\varepsilon = 4$, 7.1 kcal/mol for $\varepsilon = 24$ and 6.8 kcal/mol for $\varepsilon = 78$) lie below the ES energy (see Fig. 2). The PQQ reduction to $PQQH_2$ is accomplished. In all cases, a favorable thermodynamics of the process is retained.

The obtained PES can be compared with that of calcium containing MDH previously investigated by our group [23] considering the same mechanism. It is worthy to note that the coordination sphere of the two metal ions is different such as the charge of the metal ion, but the presence of negatively charged residues (mainly Asp and Glu in the inner coordination shell) confirms the hard nature of Lewis acid.

This striking similarity between lanthanides and Ca^{2+} ions, in terms of size, coordination environment, and ligand preferences, is widely reported in the literature [20–28].

In any case, we notice that in the previous investigation on the Ca-MDH [23], the dispersion contributions were not taken into account. Anyway, both enzymes suggest TS2 barrier as rate limiting step owing to 19.0 (Ca-MDH) and 21.4 (Ce-

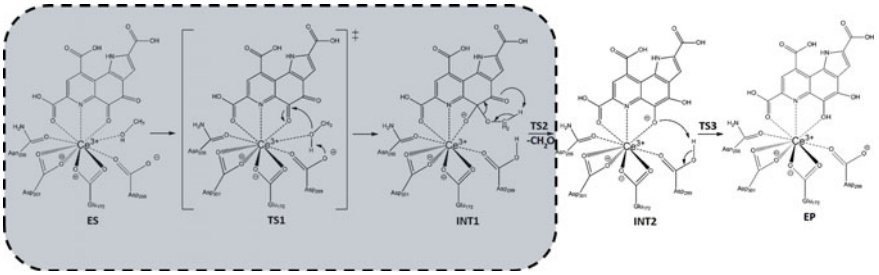

Scheme 2 Mechanism of methanol oxidation catalyzed by the Ce-MDH enzyme. The gray box evidences the mechanism's step where the metal ion is directly involved

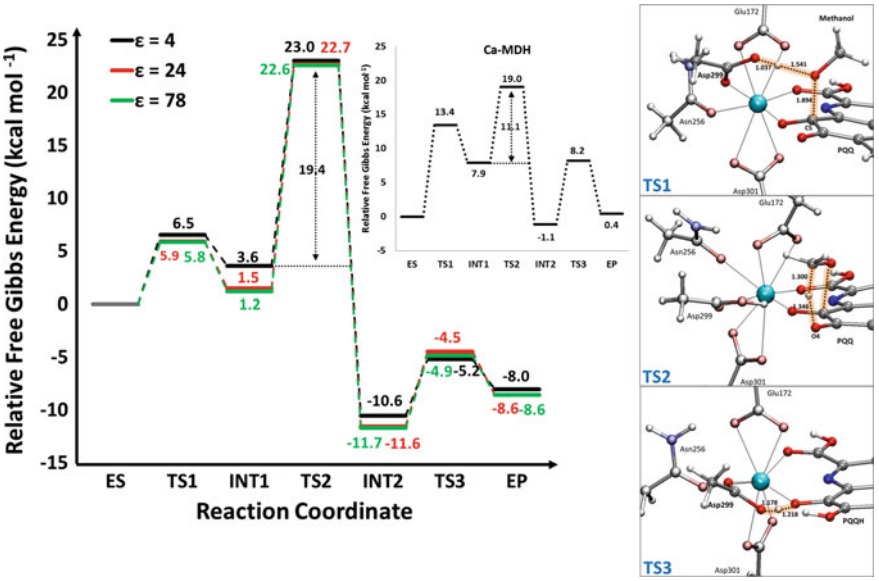

Fig. 2 Calculated energetics of methanol dehydrogenase in the Ce-MDH. The DFT energy profiles, considering three different dielectric constant values, include the electronic energy calculated at the B3LYP-D3/6-311+G(2d,2p)|SDD level of theory, ZPE, dispersion, and solvation corrections in comparison with that of Ca-MDH ($\varepsilon = 4$). In the squared boxes are depicted the optimized geometries at B3LYP-D3/6-31+G(d,p)|SDD of the three intercepted transition states. Distances are in Å

MDH) kcal/mol above the ES. This finding is indicative of a very similar catalytic activity [53].

The better catalytic activity of calcium-containing enzyme with respect to the cerium one cannot be ascribed to the stronger Lewis acidity of the Ce^{3+} since this effect influences the first step of the mechanism where the lanthanide ion makes the C5 more electrophile and intensifies the nucleophilic nature of the OH moiety in the substrate. As a consequence, the first barrier (TS1) is more favorable in Ce-MDH (3.8 kcal/mol without dispersion) than that in Ca-MDH (13.4 kcal/mol) [53].

3.2 Michaelis–Menten Complex (ES) for Ce-MDH and Eu-MDH

As the first step, with the aim to predict the catalytic activity of the Eu-MDH, a deep analysis of the catalytic pocket of Ce- and Eu-MDH arising from X-ray structures [18, 19] can give helpful hints about the metal surrounding environment entailed in the catalysis.

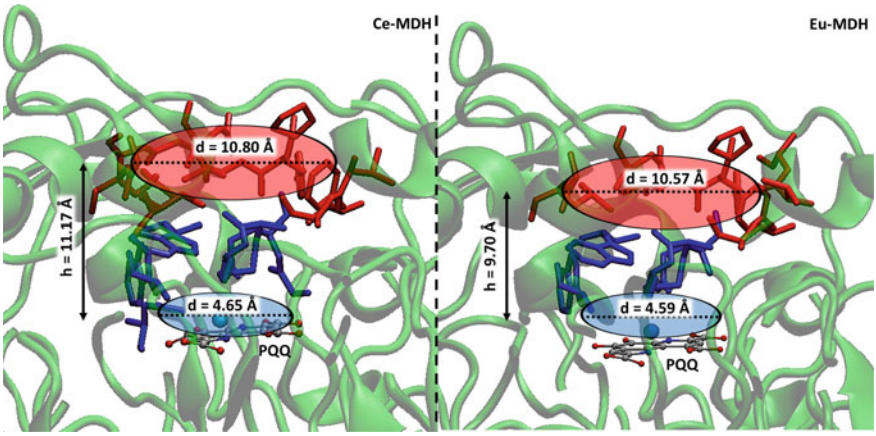

Fig. 3 Comparison of the sizes of catalytic pocket of the Ce- and Eu-MDH. In blue are indicated the hydrophilic residues (Trp260, Trp532, Cys104, Cys105, Glu172), while in red the hydrophobic ones (Eu: Pro424, Phe273, Val426, Gly427, Leu550, Ala103, Val102; Ce: Pro424, Phe273, Val426, Gly427, Leu550, Ala103, Val102; Ala101, Val100, Gly551, Ala552, Ile 535)

The crystal structure of Ce-MDH showed the active site in every monomer located in a large, deep, and conic-shaped cavity (~10.80 Å in diameter at its mouth and 11.2 Å deep). As it can be evinced from Fig. 3, in Eu-MDH, the catalytic pocket shows reduced sizes owing to 9.70 Å deep, 10.57 Å at the top, and 4.59 Å at the bottom. In both enzymes, the binding cavity of the primary CH_3OH alcohol includes a hydrophobic region at the entrance and then a hydrophilic one at the bottom. The twelve amino acid residues included in the hydrophobic region of the cerium with respect to the seven ones of europium justify the different dimensions. The "bipolar" nature of the access channel to the metal center can account for the recognition of the substrate by hydrophobic region, while the hydrophilic counterpart of the cavity in proximity to the active site comes into play during the occurrence of the reaction. This scenario in a simple way reflects the consequences due to the metal ion substitution inside the catalytic pocket owing to the slightly smaller ionic radius of europium (III) relative to cerium (III).

In the ES formation, the substrate binds to the active site, and the "complexation energy" should be an important parameter since our QM model resembles a hypothetic ML_9 species (L = oxygen atoms from the ligands).

$$ML_9 + L' \rightarrow ML_9L'$$

The total interaction energy can be computed according to equation above following the counterpoise method [58, 59] as a sum of the two-body interaction energies.

This energy represents a measure of the bond formation with the methyl alcohol by lanthanide ion increasing of the coordination number from 9 to 10. The obtained energetic values (ΔH of the above reaction) of −32.56 kcal/mol for cerium and

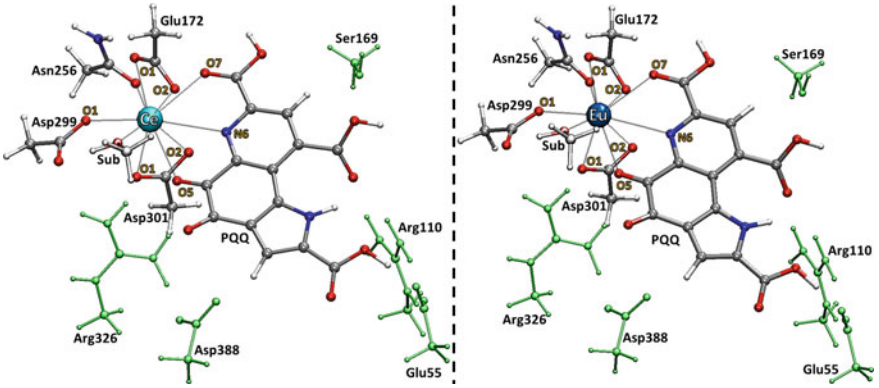

Fig. 4 Optimized geometry of the Michaelis–Menten complexes of Ce- and Eu-MDH. The amino acid residues in green belong to the outer coordination shell of the metal ions. Atoms labeled identify the first coordination shell

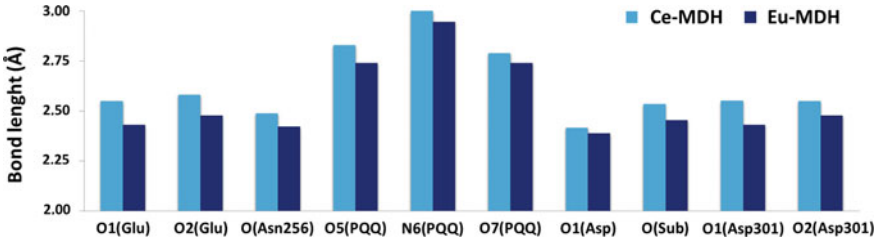

Fig. 5 Distances of the ligand atoms to metal ion in cyan for Ce-MDH and in blue for Eu-MDH. Labels of the atoms are present in Fig. 4

–31.53 kcal/mol for europium reflect as the smaller radius of the central metal the greater the non-bonding inter-ligand repulsive interactions. A possible explanation of this behavior is related to the increase in effective nuclear charge in the cerium experienced by the outer electrons (35 by ECP in Eu^{3+} vs. 30 by ECP in Ce^{3+}), essentially promoted by the incomplete shielding of the 5s and 5p electrons by the 4f ones, with consequent relativistic effects by about 10%. This result can also provide a reason for the reduced affinity constant found in the kinetic study on Eu-MDH [19].

The optimized geometries of the ES complex of Ce- and Eu-MDH are reported in Fig. 4, and the main geometrical parameters (bond distances) related to the atoms directly bonded to the metal ion are collected in Fig. 5.

Both Ce^{3+} (ionic radius 1.196 Å) and Eu^{3+} (ionic radius 1.120 Å) retain all of the amino acids in the inner coordination shell showing a coordination number equal to 9, without considering the substrate because the PQQ factor acts as a bidentate ligand. The nitrogen atom (N6) lies at 2.999 Å from the cerium in the Ce-MDH and 2.946 Å from the europium in Eu-MDH with respect to the shorter distances of M^{3+}-$O5_{PQQ}$ and M^{3+}-$O7_{PQQ}$ (see Fig. 5 and Table 1). Figure 5 clearly shows that

Table 1 Calculated coordination distances (Å) in Ca-, Ce-, and Eu-MDH in ES complexes. For comparison, the corresponding crystallographic values (Å) are reported in parenthesis

M^{n+}	$O1_{Glu172}$	$O2_{Glu172}$	O_{Asn256}	$O5_{PQQ}$	$N6_{PQQ}$	$O7_{PQQ}$	$O1_{Asp299}$	O_{Sub}	$O1_{Asp301}$	$O2_{Asp301}$
Ca^{2+}	2.426 (2.709)	2.500 (2.704)	2.414 (2.861)	2.758 (2.411)	2.787 (2.518)	2.677 (2.729)	2.379 (3.336)	2.513	–	–
Ce^{3+}	2.550 (2.667)	2.581 (2.917)	2.488 (2.715)	2.829 (2.552)	2.999 (2.800)	2.788 (2.697)	2.416 (2.857)	2.535	2.551 (2.780)	2.550 (2.469)
Eu^{3+}	2.431 (2.778)	2.478 (3.110)	2.421 (2.831)	2.740 (2.634)	2.946 (2.834)	2.74 (2.560)	2.387 (2.983)	2.454	2.431 (2.839)	2.478 (2.548)

the variation of the bond lengths in the Ce-MDH and Eu-MDH reflects the expected smooth contraction with increasing atomic number (effect of the periodicity).

A similar trend is observed even if the crystallographic distances are examined (Table 1) although they are in all the cases more elongated. In the same table are reported the coordination bonds values of the Ca-MDH that are close to those of Eu-MDH, except for the distance involving the nitrogen atom (N6) of PQQ.

In our ES optimized structure of Eu-MDH, the metal ion presents Glu172 and Asp301 in bicoordinated fashion differently from that reported in the study of Pol et al. [19]. In fact, in this work the Asp301 residue acts as unidentate ligand owing to the O1–Eu $^{3+}$ (3.842 Å) and O2-Eu^{3+} (2.359 Å) bond distances. In general, all the other coordination distances appear shorter than our ones. This probably reflects the chosen computational procedure that considers few valence electrons for the lanthanide ions [19].

The NBO analysis for the ES complexes, depicted in Fig. 6, demonstrates again a periodic trend giving in general more negative values for the cerium-containing enzyme except for some cases. A more negative charge on the substrate oxygen for the Ce-MDH with respect to the Eu-MDH is obtained. This is important for the catalytic activity because the more polarized O–H-bond of the substrate facilitates the H-transfer and the nucleophilic addition on C5 of PQQ that occurs in the first step of the reaction. In fact, the charge value on O5 atom of the PQQ cofactor retains almost the same amount in both lanthanides such as the value on C5 (0.53 |e|) not reported in the figure. This is a confirmation that the activation of the OH moiety of the methanol, and not of the PQQ cofactor, is subjected to the metal ion Lewis acidity and is crucial for the first step of the catalysis.

A further reasonable basis for evaluating the different behavior of the two Ce- and Eu-dependent methanol dehydrogenases can arise from MO energy diagram depicted in Fig. 7. Here, it is possible to observe that the energetic gap separating the HOMO from LUMO in the ES complex of Ce-MDH is smaller by 0.84 eV than that of the same orbitals in the Eu-MDH. This finding corroborates the better nature of Lewis acid of Ce^{3+} since the HOMO location on the cerium (4f orbital). In both enzymes, the LUMO lies on the PQQ cofactor that must suffer $2e^-$ reduction and is almost isoenergetic.

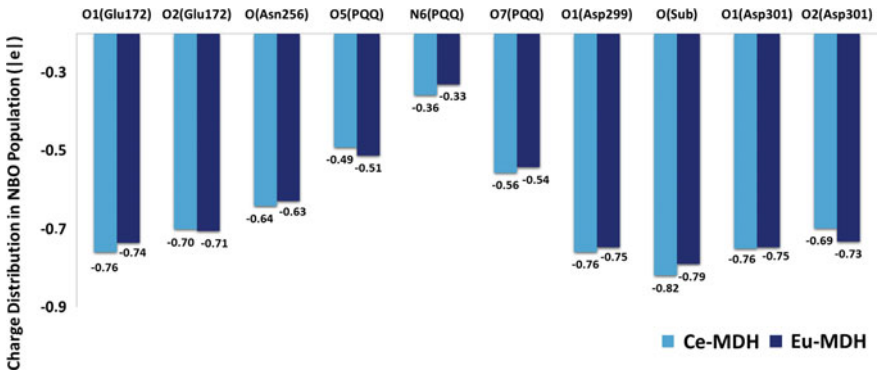

Fig. 6 NBO charges (|e|) of the coordinated atoms for ES complex of Ce-MDH and Eu-MDH

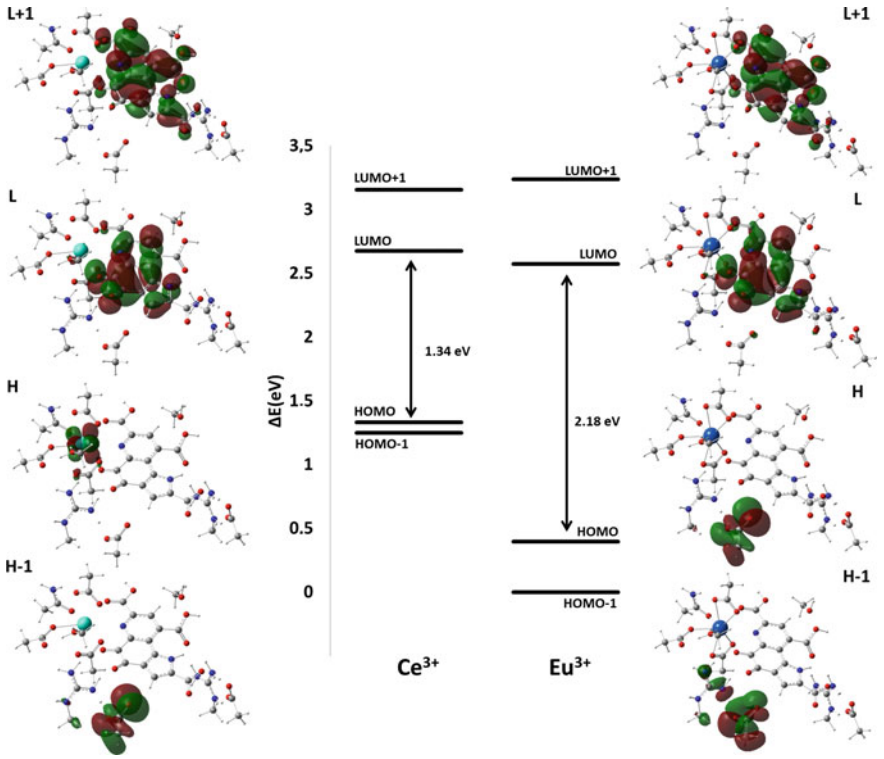

Fig. 7 Energy diagram of frontier molecular orbitals of the enzyme–substrate complexes (ES) for Ce-MDH and Eu-MDH

This behavior is different from that observed in the LUMO comparison between Ca-MDH and Ce-MDH in a previous work [55] and confirms the better Lewis acid nature of lanthanide ions.

4 Conclusions

In the present work, we have performed a theoretical investigation at QM level and using the hybrid B3LYP functional with the dispersion contribution, for giving details about the different coordination chemistry of the two considered lanthanide ions (Ce^{3+} and Eu^{3+}) in their ES complexes. The catalytic behavior of Ce-MDH as compared to Ca-MDH has been also examined. The emerged differences and similarities have been correlated to the periodic properties as atomic radius and relativistic effects (in the case of lanthanide ions).

In particular, results show that:

- PESs calculated for Ce-MDH by taking into account three diverse dielectric constant values do not suffer evident changes.
- Metal ion can play a crucial role in the activation of the methanol substrate (first step of the investigated catalytic mechanism) more than in the PQQ cofactor reduction.
- Cerium ion is a better Lewis acid than calcium and europium ones.
- Cerium more than europium acts as a better biomimetic agent for calcium-containing methanol dehydrogenase.
- Frontier orbital and NBO analysis of the enzyme–substrate complex for Ce- and Eu-MDH support the better catalytic activity of the cerium-containing enzyme.

References

1. Good NM, Vu HN, Suriano CJ, Subuyuj GA, Skovran E, Martinez-Gomez NC (2016) Pyrroloquinoline quinone ethanol dehydrogenase in Methylobacterium extorquens AM1 extends lanthanide-dependent metabolism to multicarbon substrates. J Bacteriol 198:3109–3118. https://doi.org/10.1128/JB.00478-16
2. Panichev AM (2015) Rare Earth Elements: Review of medical and biological properties and their abundance in the rock materials and mineralized spring waters in the context of animal and human geophagia reason evaluation Achiev. Life Sci 9:95–103. https://doi.org/10.1016/j.als.2015.12.001
3. Brittain HG, Richardson FS, Martin RB (1976) Terbium(III) emission as a probe of calcium(II) binding sites in proteins. J Am Chem Soc 98:8255–8260. https://doi.org/10.1021/ja00441a060
4. Martin RB, Richardson F (1979) Lanthanides as probes for calcium in biological systems. Q Rev Biophys 12:181–209. https://doi.org/10.1017/S0033583500002754
5. Chistoserdova L (1996) Metabolism of formaldehyde in M. extorquens AM1. Molecular genetic analysis and mutant characterization. In: Lidstrom ME, Tabita FR (eds) Microbial growth on C1 compounds. Kluwer Academic Publishers, Dordrecht, pp 16–24
6. Harms N, Ras J, Koning S, Reijinders WNM, Stouthamer AH, van Spanning RJM (1996) Genetics of C1 metabolism regulation in Paracoccus denitrificans. In: Lidstrom ME, Tabita

FR (eds) Microbial growth on C1 compounds. Kluwer Academic Publishers, Dordrecht, pp 126–132
7. Hibi Y, Asai K, Arafuka H, Hamajima M, Iwama T, Kawai K (2011) Molecular structure of La^{3+}-induced methanol dehydrogenase-like protein in Methylobacterium radiotolerans. J Biosci Bioeng 111:547–549. https://doi.org/10.1016/j.jbiosc.2010.12.017
8. Chistoserdova L (2016) Lanthanides: new life metals? World J Microbiol Biotechnol 32:138. https://doi.org/10.1007/s11274-016-2088-2
9. Anthony C (2000) Methanol dehydrogenase, a PQQ-containing quinoprotein dehydrogenase. In: Holzenburg A, Scrutton NS (eds) Enzyme-catalyzed electron and radical transfer, vol 35. Springer, New York
10. Anthony C (2004) The quinoprotein dehydrogenases for methanol and glucose. Arch Biochem Biophys 428:2–9. https://doi.org/10.1016/j.abb.2004.03.038
11. Goodwin PM, Anthony C (1998) The biochemistry, physiology and genetics of PQQ and PQQ-containing enzymes. Adv Microb Physiol 40:1–80. https://doi.org/10.1016/S0065-2911(08)60129-0
12. Cotton S (2006) Lanthanide and actinide chemistry. Wiley, Chichester; Evans CH (1990) Biochemistry of the lanthanides. Springer, New York
13. Shiller AM, Chan EW, Joung DJ, Redmond MC, Kessler JD (2017) Light rare earth element depletion during Deepwater Horizon blowout methanotrophy. Sci Rep 7:1–9. https://doi.org/10.1038/s41598-017-11060-z
14. Vu HN, Subuyuj GA, Vijayakumar S, Good NM, Martinez-Gomez NC, Skovran E (2016) Lanthanide-dependent regulation of methanol oxidation systems in Methylobacterium extorquensAM1 and their contribution to methanol growth. J Bacteriol 198:1250–1259. https://doi.org/10.1128/JB.00937-15
15. Ochsner AM, Sonntag F, Buchhaupt M, Schrader J, Vorholt JA (2015) Methylobacterium extorquens: methylotrophy and biotechnological applications. Appl Microbiol Biotechnol 99:517–534. https://doi.org/10.1007/s00253-014-6240-3
16. Semrau JD, Di Spirito AA, Gu W, Yoon S (2018) Metals and methanotrophy. Appl Environ Microbiol 84:e02289–17. https://doi.org/10.1128/AEM.02289-17
17. Pol A, Barends TRM, Dietl A, Khadem AF, Eygensteyn J, Jetten MSM, Op den Camp HJM (2014) Rare earth metals are essential for methanotrophic life in volcanic mudpots. Environ Microbiol 16:255–264. https://doi.org/10.1111/1462-2920.12249
18. Afolabi PR, Mohammed F, Amaratunga K, Majekodunmi O, Dales L, Gill R, Thompson D, Cooper B, Wood P, Goodwin M, Anthony C (2001) Site-directed mutagenesis and X-ray crystallography of the PQQ-containing quinoprotein methanol dehydrogenase and its electron acceptor, cytochrome cL. Biochemistry 40:9799–9809. https://doi.org/10.1021/bi0029321
19. Jahn B, Pol A, Lumpe H, Barends TRM, Dietl A, Hogendoorn C, Op den Camp HJM, Daumann LJ (2018) Similar but not the same: first kinetic and structural analyses of a methanol dehydrogenase containing a europium ion in the active site. ChemBioChem 19:1147–1153. https://doi.org/10.1002/cbic.201800130
20. Zheng YJ, Bruice TC (1997) Conformation of coenzyme pyrroloquinoline quinone and role of Ca^{2+} in the catalytic mechanism of quinoprotein methanol dehydrogenase. PNAS 94:11881–11886. https://doi.org/10.1073/pnas.94.22.11881
21. Zheng YJ, Xia Z, Chen Z, Mathews FS, Bruice TC (2001) Catalytic mechanism of quinoprotein methanol dehydrogenase: a theoretical and X-ray crystallographic investigation. PNAS 98:432–434. https://doi.org/10.1073/pnas.98.2.432
22. Idupulapati NB, Mainardi DS (2010) Quantum chemical modeling of methanol oxidation mechanisms by methanol dehydrogenase enzyme: effect of substitution of calcium by barium in the active site. J Phys Chem A 114:1887–1896. https://doi.org/10.1021/jp9083025
23. Leopoldini M, Russo N, Toscano M (2007) The preferred reaction path for the oxidation of methanol by PQQ-containing methanol dehydrogenase: addition-elimination versus hydride-transfer mechanism. Chem Eur J 13:2109–2117. https://doi.org/10.1002/chem.200601123
24. Hothi P, Sutcliffe MJ, Scrutton NS (2005) Kinetic isotope effects and ligand binding in PQQ-dependent methanol dehydrogenase. Biochem J 388:123–133. https://doi.org/10.1042/BJ20041731

25. Zheng X, Reddy SY, Bruice TC (2007) Mechanism of methanol oxidation by quinoprotein methanol dehydrogenase. PNAS 104:745–749. https://doi.org/10.1073/pnas.0610126104
26. Reddy SY, Bruice TC (2004) Determination of enzyme mechanisms by molecular dynamics: studies on quinoproteins, methanol dehydrogenase, and soluble glucose dehydrogenase. Protein Sci 13:1965–1978 (2004). https://doi.org/10.1110/ps.04673404
27. Idupulapati NB, Mainardi DS (2009) THEOCHEM 901:72–80. https://doi.org/10.1016/j.theochem.2009.01.004
28. McSkimming A, Cheisson T, Carroll PJ, Schelter EJ (2018) Functional synthetic model for the lanthanide-dependent quinoid alcohol dehydrogenase active site. J Am Chem Soc 140:1223–1226. https://doi.org/10.1021/jacs.7b12318
29. Nakagawa T, Mitsui R, Tani A, Sasa K, Tashiro S, Iwama T, Hayakawa T, Kawai K (2012) A catalytic role of XoxF1 as La3+-dependent methanol dehydrogenase in Methylobacterium extorquens strain AM1. PLoS ONE 7:e50480. https://doi.org/10.1371/journal.pone.0050480
30. Chu F, Beck DAC, Lidstrom ME (2016) MxaY regulates the lanthanide-mediated methanol dehydrogenase switch in Methylomicrobium buryatense. PeerJ 4:e2435. https://doi.org/10.7717/peerj.2435
31. Skovran E, Martinez-Gomez NC (2015) Just add lanthanides. Science 348:862–863. https://doi.org/10.1126/science.aaa9091
32. Blomberg RMA, Borowski T, Himo F, Liao R-Z, Siegbahn PEM (2014) Quantum chemical studies of mechanisms for metalloenzymes. Chem Rev 114:3601–3658, and references therein. https://doi.org/10.1021/cr400388t
33. Piazzetta P, Marino T, Russo N (2014) Promiscuous ability of human carbonic anhydrase: QM and QM/MM Investigation of carbon dioxide and carbodiimide hydration. Inorg Chem 53:3488–3493. https://doi.org/10.1021/ic402932y
34. Amata O, Marino T, Russo N (2011) Catalytic activity of a ζ-class zinc and cadmium containing carbonic anhydrase. Compared work mechanisms. Phys Chem Chem Phys 13:3468–3477. https://doi.org/10.1039/C0CP01053G
35. Liao R-Z, Yu G, Himo F (2010) Mechanism of tungsten-dependent acetylene hydratase from quantum chemical calculations. PNAS 107:22523–22527. https://doi.org/10.1073/pnas.1014060108
36. Ramos MJ, Fernandes PA (2008) Computational enzymatic catalysis. Acc Chem Res 41:689–698. https://doi.org/10.1021/ar7001045
37. Marino T, Russo N, Toscano M (2012) Catalytic mechanism of the arylsulfatase promiscuous enzyme from pseudomonas aeruginosa. Chem Eur J 19:2185–2192. https://doi.org/10.1002/chem.201201943
38. Gaussian 09, Revision D.01, Frisch MJ, Trucks GW, Schlegel HB, Scuseria GE, Robb MA, Cheeseman JR, Scalmani G, Barone V, Mennucci B, Petersson GA, Nakatsuji H, Caricato M, Li X, Hratchian HP, Izmaylov AF, Bloino J, Zheng G, Sonnenberg JL, Hada M, Ehara M, Toyota K, Fukuda R, Hasegawa J, Ishida M, Nakajima T, Honda Y, Kitao O, Nakai H, Vreven T, Montgomery Jr JA, Peralta JE, Ogliaro F, Bearpark M, Heyd JJ, Brothers E, Kudin KN, Staroverov VN, Keith T, Kobayashi R, Normand J, Raghavachari K, Rendell A, Burant JC, Iyengar SS, Tomasi J, Cossi M, Rega N, Millam JM, Klene M, Knox JE, Cross JB, Bakken V, Adamo C, Jaramillo J, Gomperts R, Stratmann RE, Yazyev O, Austin AJ, R. Cammi R, Pomelli C, Ochterski JW, Martin RL, Morokuma K, Zakrzewski VG, Voth GA, Salvador P, Dannenberg JJ, Dapprich S, Daniels AD, Farkas O, Foresman JB, Ortiz JV, Cioslowski J, Fox DJ (2013) Gaussian, Inc., Wallingford, CT
39. Lee C, Yang W, Parr RG (1988) Development of the Colle-Salvetti correlation-energy formula into a functional of the electron density. Phys Rev B 37:785–789. https://doi.org/10.1103/PhysRevB.37.785
40. Becke AD (1993) Density-functional thermochemistry. III. The role of exact exchange. J Chem Phys 98:5648–5652. https://doi.org/10.1063/1.464913
41. Andrae D, Haußermann H, Dolg M, Stoll H, Preuß H (1990) Energy-adjustedab initio pseudopotentials for the second and third row transition elements. Theor Chim Acta 77:123–141. https://doi.org/10.1007/BF01114537

42. Grimme S, Ehrlich S, Goerigk L (2011) Effect of the damping function in dispersion corrected density functional theory. J Comput Chem 32:1456–1465. https://doi.org/10.1002/jcc.21759
43. Cossi M, Rega N, Scalamani V, Barone V (2003) Energies, structures, and electronic properties of molecules in solution with the C-PCM solvation model. J Comput Chem 24:669–681. https://doi.org/10.1002/chem.201700381
44. Barone V, Cossi M (1998) Quantum calculation of molecular energies and energy gradients in solution by a conductor solvent model. J Phys Chem A 102:1995–2001. https://doi.org/10.1021/jp9716997
45. Chen W, Fang WH, Himo F (2009) Reaction mechanism of the binuclear zinc enzyme glyoxalase II—a theoretical study. J Inorg Biochem 103:274–281. https://doi.org/10.1016/j.jinorgbio.2008.10.016
46. Ziao RZ, Himo F Yu JG, Liu RZ (2010) Dipeptide hydrolysis by the dinuclear zinc enzyme human renal dipeptidase: mechanistic insights from DFT calculations. J Inorg Biochem 104:37–46. https://doi.org/10.1016/j.jinorgbio.2009.09.025
47. Sousa SF, Fernandes PA, Ramos MJ (2009) The search for the mechanism of the reaction catalyzed by farnesyltransferase. Chem Eur J 15:4243–4247. https://doi.org/10.1002/chem.200802745
48. Alberto ME, Marino T, Ramos MJ, Russo N (2010) Atomistic details of the catalytic mechanism of Fe(III)–Zn(II) purple acid phosphatase. J Chem Theory Comput 6:2424–2433. https://doi.org/10.1021/ct100187c
49. Siegbahn PEM, Eriksson LA, Himo F, Pavlov M (1998) Hydrogen atom transfer in ribonucleotide reductase (RNR). J Phys Chem B 102:10622–10629. https://doi.org/10.1021/jp9827835
50. Warshel A (1991) Computer modeling of chemical reactions in enzymes and solutions. Wiley, New York
51. Piazzetta P, Marino T, Russo N (2014) Insight into the promiscuous activity of human carbonic anhydrase against the cyanic acid substrate from a combined QM and QM/MM investigation. Phys Chem Chem Phys 16:16671–16676. https://doi.org/10.1039/C4CP02363C
52. Ribeiro AJM, Alberto ME, Ramos MJ, Fernandes PA, Russo N (2013) The catalytic mechanism of protein phosphatase 5 established by DFT calculations. Chem Eur J 114:3601–3658. https://doi.org/10.1002/chem.201301565
53. Prejanò M, Marino T, Russo N (2017) How can methanol dehydrogenase from Methylacidiphilum fumariolicum work with the alien CeIII ion in the active center? A theoretical study. Eur Chem J 23:8652–8657. https://doi.org/10.1002/chem.201700381
54. Prejanò M, Marino T, Rizzuto C, Madrid JCM, Russo N, Toscano M (2017) Reaction mechanism of low-spin iron(III)- and cobalt(III)-containing nitrile hydratases: a quantum mechanics investigation. Inorg Chem 56:13390–13400. https://doi.org/10.1021/acs.inorgchem.7b02121
55. Bogart JA, Lewis AJ, Schelter EJ (2015) DFT study of the active site of the XoxF-type natural, cerium-dependent methanol dehydrogenase enzyme. Chem Eur J 21:1743–1748. https://doi.org/10.1002/chem.201405159
56. E. D. Glendening, A. E. Reed, J. E. Carpenter, F. Weinhold, NBO, version 3.1
57. Anthony C (1996) Quinoprotein-catalysed reactions. Biochem J 320:697–711. https://doi.org/10.1042/bj3200697
58. Simon S, Duran M, Dannenberg JJ (1996) How does basis set superposition error change the potential surfaces for hydrogen-bonded dimers? J Phys Chem 105:11024–11031. https://doi.org/10.1063/1.472902
59. Boys SF, Bernardi F (1970) The calculation of small molecular interactions by the differences of separate total energies. Some procedures with reduced errors. Mol Phys 19:553–566. https://doi.org/10.1080/00268977000101561